Research Square

Preprints are preliminary reports that have not undergone peer review.
They should not be considered conclusive, used to inform clinical practice,
or referenced by the media as validated information.

Structure-Based Virtual Screening Identifies Fumaric Acid as an MD2-Pocket-Associated Candidate That Attenuates LPS-Induced Inflammatory Responses in Human PBMCs

Mobina Azimi
University of Zanjan
Abbas Bahari
bahari@znu.ac.ir
University of Zanjan
Bahram Maleki
University of Zanjan
Milad Lagzian
University of Sistan and Baluchistan
Mahdi Tavakolizadeh
Alborz University of Medical Sciences
Davood Koolivand
University of Zanjan
Parsa Dorani
University of Zanjan
Elahe Gholamian
University of Zanjan
Fatemeh S eyed Monfared Zanjani
University of Zanjan
Fatemeh Najafi
Zabol University

Article

Keywords: Toll-like receptor 4 (TLR4), Myeloid differentiation factor 2 (MD2), Structure-based virtual screening (SBVS), Fumaric acid

Posted Date: November 24th, 2026

DOI: https://doi.org/10.21203/rs.3.rs-11566926/v1

License: This work is licensed under a Creative Commons Attribution 4.0 International License.
Read Full License

Additional Declarations: No competing interests reported.

Structure-Based Virtual Screening Identifies Fumaric Acid as an MD2-Pocket-Associated Candidate That Attenuates LPS-Induced Inflammatory Responses in Human PBMCs

Mobina Azimi[1], Abbas Bahari[2*], Bahram Maleki[1], Milad Lagzian[3], Mahdi Tavakolizadeh[4,5*], Davood Kolivand[1], Parsa Dorani[6], Elahe Gholamiavaian[2], Fatemeh Seyed Monfared Zanjani[6], Fatemeh Najafi[7]

1 Department of Agronomy, Faculty of Agriculture, University of Zanjan, Iran

2 Research Institute of modern biological techniques, University of Zanjan, Iran

3 Department of Biology, Faculty of science, University of Sistan and Baluchistan, Iran

4 Evidence-based Phytotherapy and Complementary Medicine Research Center, Alborz University of Medical Sciences, Karaj, Iran.

5 Department of Pharmacognosy, School of Pharmacy, Zanjan University of Medical Sciences, Zanjan, Iran.

6 Department of Biology, Faculty of Science, University of Zanjan, Zanjan, Iran

7 Department of Biology, Faculty of Science, University of Zabol, Iran

corresponding authors:

- Abbas Bahari: Bahari@znu.ac.ir, ORCID: 0000-0003-1913-4837
- Mahdi Tavakolizadeh: mahdi_tavakoli@yahoo.com, ORCID: 0000-0002-1406-8634

Abstract

Toll-like receptor 4 (TLR4) signaling, initiated by lipopolysaccharide (LPS) recognition at the TLR4/MD2 interface, drives innate inflammatory gene programs and is a critical pathological node across infectious and sterile inflammatory states. Structural characterization has established that ligand occupancy and conformational control within the MD2 hydrophobic pocket dictate receptor dimerization and downstream nuclear factor-κB (NF-κB)-linked transcription; however, the clinical translation of direct TLR4/MD2 antagonists has been hampered by inconsistent efficacy in heterogeneous patient populations. In this study, we investigated whether a chemically simple, metabolite-like scaffold could be prioritized from a vast natural product library using a stringent, multi-platform structure-based virtual screening workflow and subsequently validated in primary human immune cells. Utilizing the crystal structure of the TLR4/MD2/LPS complex (PDB ID: 4G8A) as a structural template, we deployed a sequential filtering strategy to screen over 57,000 compounds. Multi-engine consensus docking identified fumaric acid as a reproducible hit, while hierarchical clustering characterized structural relationships among the prioritized candidates. Molecular dynamics simulations (100 ns) indicated dynamic accommodation of fumaric acid within the MD2 pocket, compatible conformational adaptation of the MD2 binding region, and negative protein–ligand interaction energies, while hydrophobic surface mapping showed relocation of the ligand from the cavity entrance into the pocket with local rearrangement of surrounding residues. Empirically, functional validation in human peripheral blood mononuclear cells (PBMCs) demonstrated that fumaric acid attenuated LPS-induced transcriptional up-regulation in a concentration-dependent but gene-specific manner (*IL1B* mainly at 10 ng/mL and *NFKB1* at 100 ng/mL, with no significant reduction of *TNF* transcripts) and reduced IL-1β and TNF-α secretion. Collectively, these findings position fumaric acid as a structurally supported, MD2-pocket-associated candidate and a tractable chemical probe for interrogating target pocket plasticity, while remaining agnostic regarding clinical efficacy and definitive therapeutic antagonism.

Keywords: Toll-like receptor 4 (TLR4), Myeloid differentiation factor 2 (MD2), Structure-based virtual screening (SBVS), Fumaric acid

1. Introduction

Innate immunity is the first line of host defense. It recognizes invading microbes and cellular damage quickly and so maintains homeostasis[1-3]. Pattern recognition receptors (PRRs) detect conserved microbial structures called

pathogen-associated molecular patterns, and also endogenous damage-associated molecular patterns released from injured tissue [4-6]. Under normal conditions inflammation is tightly regulated to clear infection and support tissue repair, but excessive or poorly controlled activation releases pro-inflammatory mediators without restraint[1, 5, 6]. Excessive systemic inflammation contributes to life-threatening conditions such as sepsis, which carries substantial global morbidity and mortality[1, 7]. Persistent low-grade inflammation also drives progressive tissue damage in autoimmune, neurodegenerative, cardiovascular and age-associated disorders [3, 5]. Treating dysregulated inflammation therefore starts with understanding how PRR signaling is controlled[1, 3].

Among PRRs, Toll-like receptor 4 (TLR4) is a major transmembrane sensor for lipopolysaccharide (LPS), the principal endotoxic glycolipid of the Gram-negative outer membrane[4, 7, 8]. TLR4 alone recognizes LPS poorly and depends on the co-receptor myeloid differentiation factor-2 (MD2), which binds the extracellular domain of TLR4 [2, 9]. During Gram-negative infection, LPS-binding protein and CD14 transfer LPS to the TLR4/MD2 complex, and recognition of the lipid A moiety promotes receptor dimerization and formation of the active $[TLR4/MD2/LPS]_2$ complex[3, 7]. Dimerization brings the intracellular Toll/interleukin-1 receptor (TIR) domains together and starts two pathways. One is the myeloid differentiation primary response 88 (MyD88)-dependent pathway at the plasma membrane. The other is the TIR domain-containing adaptor inducing interferon-β (TRIF)-dependent pathway, which follows CD14-dependent internalization of the receptor[3, 4, 10]. In the MyD88 pathway, TIR domain-containing adaptor protein (TIRAP) and MyD88 are recruited and activate the IκB kinase complex. This activates nuclear factor-κB (NF-κB), which drives transcription of inflammatory genes including interleukin-1 beta (*IL1B*) and tumor necrosis factor (*TNF*)[4, 5, 10].

Structural studies show that MD2 has a β-cup fold with a deep hydrophobic cavity that holds the lipid A component of LPS[3, 7, 11]. In the agonist complex the acyl chains of lipid A fill the cavity, and one chain exposed at the entrance contacts the neighboring TLR4 molecule and promotes dimerization. Competitive antagonists such as Eritoran sit in the cavity in a different orientation, which prevents productive dimerization and downstream signaling[6, 8, 11]. Despite many efforts to target the TLR4/MD2 axis, clinical translation has been difficult. The synthetic lipid A antagonist Eritoran, for example, did not improve survival in a multinational Phase III trial in severe sepsis[3, 8, 12]. Lipid A mimetics (including disaccharide mimetics) and small-molecule TLR4 inhibitors such as TAK-242 have also run into problems with chemical complexity, synthesis, pharmacokinetics, species-dependent responses or safety[6,

8]. *Plant-derived compounds have also been tested. Atractylenolide I, a sesquiterpene lactone from the rhizome of* Atractylodes macrocephala, was reported to inhibit TLR4 signaling by interfering with LPS binding to TLR4 on human leukocytes[13]. Chemically diverse, non-lipid small molecules that act on the MD2 binding region and influence TLR4 signaling are still needed[3, 4, 8].

Computer-aided drug discovery, including structure-based virtual screening (SBVS) and molecular docking, makes it efficient to search large chemical libraries and prioritize compounds that may bind a receptor[3, 14]. SBVS uses experimentally resolved three-dimensional protein structures to predict ligand orientations and evaluate candidates within functional binding sites, including the MD2 cavity[3, 4, 14]. A single docking scoring function, however, rests on simplified empirical and force-field approximations that represent electrostatics, desolvation and entropy poorly, so it can produce false positives or wrong rankings[14]. Consensus docking, which combines several algorithms, rescoring strategies and pharmacophore-based filtering, reduces dependence on any one scoring function and increases confidence in the ranking[3, 14]. Molecular dynamics (MD) simulations add information on time-dependent conformational flexibility, including loop adaptability, and on how predicted ligand-protein complexes behave in explicit solvent[3, 6, 14]. Docking and MD give a structural prioritization and a test of dynamic compatibility. Neither establishes direct binding or biological efficacy, so experimental validation is required[3, 4, 14].

Immunometabolism, a parallel line of research, has drawn attention to endogenous metabolic intermediates that regulate inflammation[3, 4]. Fumarate, an intermediate of the tricarboxylic acid cycle, has recognized immunomodulatory properties, and its lipophilic ester dimethyl fumarate (DMF) is used clinically in neuroinflammatory and autoimmune conditions such as multiple sclerosis[3]. Fumaric acid and DMF are chemically distinct: fumaric acid is an unesterified, hydrophilic dicarboxylic acid, and the ester groups of DMF change its biological properties substantially[4]. Fumaric acid is compact, and its carboxylate groups can form polar and electrostatic interactions, which makes it a candidate for computational study of interactions within functionally relevant regions of MD2[4].

Identifying chemically diverse small molecules that influence LPS-associated inflammatory responses remains challenging despite extensive work on TLR4/MD2 biology and ligand-based approaches. We screened more than 57,000 compounds from a traditional Chinese medicine (TCM) database[15] against the LPS-binding region of MD2 using Glide HTVS, SP, and XP docking. The top-ranked candidates were further evaluated using three additional

docking platforms (MOE, ICM-Pro, and CLC Drug Discovery Workbench), clustered based on structural similarity, and subjected to 100 ns molecular dynamics simulations in complex with TLR4/MD2, using atractylenolide I as the reference ligand system. The prioritized compound was subsequently evaluated in LPS-stimulated primary human peripheral blood mononuclear cells (PBMCs) by measuring *IL1B*, *TNF*, and *NFKB1* expression and cytokine secretion. This workflow prioritized fumaric acid as an MD2-pocket-associated candidate. The aim was to identify a plant-derived small molecule predicted to associate with the LPS-binding region of MD2 and evaluate its ability to modulate LPS-induced inflammatory responses.

2. Materials and Methods

This study involving human PBMCs was conducted in accordance with the Declaration of Helsinki and its subsequent amendments. The experimental protocols were reviewed and approved by the Institutional Review Board (Ethics Committee) of the University of Zanjan (ethics approval code IR.ZNU.REC.1402.008). All participants gave written informed consent before sample collection.

2.1. Study design

The study had three phases. First, more than 57,000 compounds from the TCM Database@Taiwan[15] were docked into the LPS-binding cavity of MD2 (PDB ID: 4G8A) using Glide HTVS, SP and XP in Schrödinger 2015. The top-ranked compounds were re-docked in MOE, ICM-Pro and CLC Drug Discovery Workbench and clustered by structural similarity. One lead was selected from the ten by the criteria in Section 2.4. Second, 100 ns MD simulations were run in NAMD 2.13 integrated into MOE2018 for three systems: TLR4/MD2 with fumaric acid, TLR4/MD2 with atractylenolide I as the reference ligand, and the apo TLR4/MD2 complex. Snapshots from the start of the simulation and after relocation of fumaric acid were shown on a hydrophobicity-colored MD2 surface to follow the position of the ligand in the pocket. Third, fumaric acid was tested in LPS-stimulated primary human PBMCs by qPCR for *IL1B*, *TNF* and *NFKB1* and by ELISA for IL-1β and TNF-α secretion (Figure 1, in which the three phases are shown as four workflow modules).

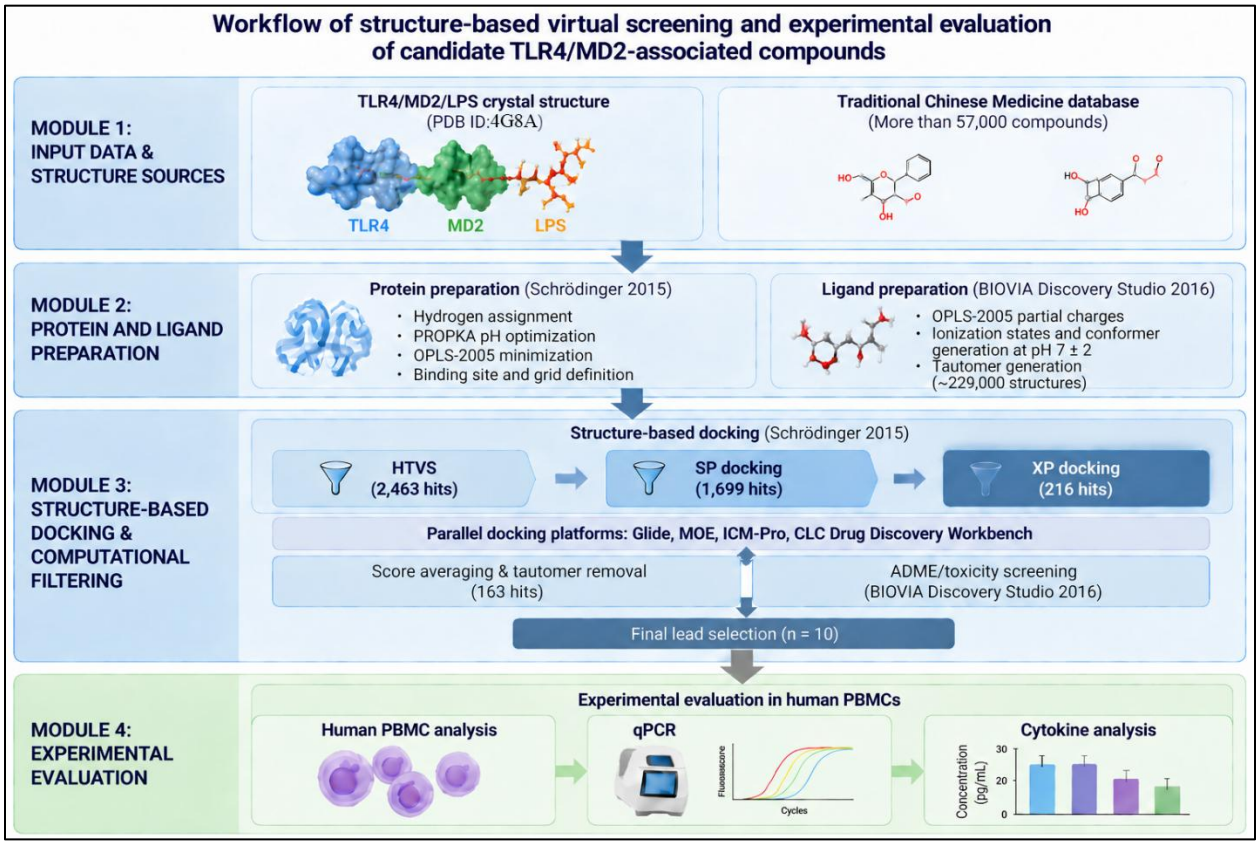

Figure 1. Integrated computational–experimental workflow for identification and evaluation of candidate MD2-pocket-associated compounds. The workflow illustrates four sequential modules: input structure and compound library selection, protein and ligand preparation, structure-based virtual screening and consensus-based computational prioritization, and ex vivo evaluation in human peripheral blood mononuclear cells (PBMCs). The TLR4/MD2/LPS crystal structure (PDB ID: 4G8A) was used as the structural target, and compounds from the Traditional Chinese Medicine database were processed through sequential high-throughput screening (HTVS), standard precision (SP), and extra precision (XP) docking, followed by cross-platform evaluation using Glide, MOE, ICM-Pro, and CLC Drug Discovery Workbench. The final prioritized candidates were assessed through molecular dynamics simulations and PBMC-based analyses including quantitative PCR and cytokine secretion measurements.

2.2. Structural Preparation of the TLR4/MD2 Receptor Template

The crystal structure of human TLR4/MD2 bound to LPS (PDB ID: 4G8A, resolution 2.4 Å) was taken from the Protein Data Bank[2]. The entry carries the TLR4 polymorphisms D299G and T399I. It was prepared with the Protein

Preparation Wizard in Schrödinger 2015. Bond orders were assigned and corrected, and hydrogens were added. Water molecules beyond 5 Å from the native ligands were deleted. PROPKA set the protonation states at pH 7.2. The structure was then minimized with the OPLS_2005 force field, and the native LPS ligands were removed before docking.

The docking grid was generated with constraints on three MD2 residues, Arg90, Ser118 and Ser120, which lie at the rim of the LPS-binding pocket and take part in LPS recognition[6, 7]. This region is the main LPS–MD2 interface, and a compound that binds here could interfere with LPS-induced TLR4 signaling.

2.3. Formulation and Optimization of the Ligand Library

The initial ligand library comprised more than 57,000 compounds from the TCM Database@Taiwan[15]. The structures were supplied as three-dimensional SDF files and prepared with LigPrep in Schrödinger 2015. Hydrogen atoms were added, protonation and ionization states were generated at pH 7.0, and problematic structures and ions were removed. Up to 32 tautomers were generated per compound, and the conformers were minimized with the OPLS_2005 force field. The preparation produced approximately 220,000 three-dimensional structures for virtual screening.

2.4. Multi-Platform Molecular Docking and Consensus Strategy

The prepared ligand library (Section 2.3) was docked into the MD2 LPS-binding region with Glide in Schrödinger 2015[16], using the constrained grid from Section 2.2. Docking ran in three sequential modes: high-throughput virtual screening (HTVS), standard precision (SP) and extra precision (XP), with increasingly strict sampling and scoring. Ligand van der Waals radii were scaled by 1.0, the partial-charge cutoff was 0.25, and one pose was kept per ligand. HTVS passed 2,463 candidates to SP, SP passed 1,699 to XP, and 216 leads remained after XP.

The XP leads were then re-docked in MOE 2017[17], ICM-Pro 3.8.6[18], and CLC Drug Discovery Workbench 4.0[19]. These programs differ in their algorithms, input requirements and scoring functions, so receptor preparation, binding-site definition and docking were done separately in each one, all targeting the same MD2 LPS-binding region. For every candidate, the best-scoring pose from each program was kept.

The scores from Schrödinger, MOE, ICM-Pro and CLC stayed on their own scales, and their arithmetic mean was used to rank the leads. Because the scales are not directly comparable, the averages served only to prioritize candidates and are not estimates of binding affinity. Duplicate tautomers were removed, and the top-ranked compounds were checked against Lipinski's rule of five and ADME/toxicity properties in BIOVIA Discovery Studio 2017. Ten leads passed this filter.

Candidate sets for the Venn diagram were the selected compounds with higher scores in each of the three re-docking programs (MOE, ICM-Pro and CLC). One of the ten leads was chosen for experimental testing based on its presence in all three candidate sets (Figure 2), together with its consistent prioritization across the docking platforms and the lowest cross-platform score variability among the ten leads (Table 2).

2.5. Hierarchical Clustering by Structural Similarity

The ten leads were clustered by structural similarity in ICM-Pro. LPS, the native TLR4/MD2 agonist, and Eritoran, a synthetic lipid A analog with TLR4 antagonist activity, were included as structural references. Clustering was hierarchical, using the unweighted pair group method with arithmetic mean (UPGMA), and the result is shown as a dendrogram.

2.6. Interaction analysis of the docked pose

The docked pose of fumaric acid in the TLR4/MD2 complex was analyzed using Schrödinger Maestro 2018-2. Two-dimensional ligand interaction diagrams were generated for fumaric acid and, as a structural reference, for the native LPS ligand in the TLR4/MD2/LPS crystal structure (PDB ID: 4G8A; Figure 3). The fumaric acid docked pose was also inspected in three dimensions relative to the MD2 cavity to evaluate ligand orientation and its position relative to surrounding residues. The fumaric acid pose was taken directly from the docking output without manual modification, whereas the LPS pose was obtained from the crystallographic structure.

Three-dimensional molecular visualization was performed to assess the spatial orientation, cavity positioning, and steric complementarity of the selected compound at the receptor pocket (Figure 4). Analysis focused specifically on residues lining the canonical lipid A-binding cavity. region of the cavity, contributing to the predicted ligand accommodation within the pocket. Interaction geometries were obtained directly from docking outputs without manual structural optimization or post hoc realignment.In the starting pose, Ser118 (side chain), Phe119 (backbone) and Ser120 (backbone) were predicted to form hydrogen-bond interactions with the ionized carboxylate oxygen atoms of

fumaric acid (Figure 4B). In the interaction diagram of the docked pose, Ser120 and Arg264 (TLR4) formed hydrogen bonds, and Phe119 contributed hydrophobic contacts (Figure 3A). Additional hydrophobic contacts were observed with adjacent side chains lining the inner

2.7. Explicit-Solvent Molecular Dynamics Simulations

To evaluate the dynamic behavior of the docked complexes beyond static docking predictions, molecular dynamics (MD) simulations were performed using NAMD 2.13 integrated into MOE 2018. Three TLR4/MD2 systems were simulated under identical conditions: the unliganded TLR4/MD2 complex (TLR4-empty), the atractylenolide-I-bound reference complex (TLR4-Ref), and the fumaric acid-bound TLR4/MD2 complex (TLR4-FUMA).

The simulations were performed according to an established NAMD simulation protocol described previously[20]. The Amber10EHT all-atom force field was used for potential energy calculations throughout the simulation steps. Each system was solvated in a cubic water box using the TIP3 water model with a 5 Å distance between the solute and the periodic boundary. Counterions were added to neutralize the systems.

Each system underwent energy minimization for 1 ns, followed by heating to 300 K for 5 ns and equilibration for 10 ns. The production phase was performed for 100 ns under the NPT ensemble. Trajectory frames were sampled every 2 ps and analyzed for backbone root-mean-square deviation (RMSD) changes and protein–ligand interaction energy profiles.

2.8. Hydrophobic Surface Mapping and Pocket Accommodation Analysis

To visualize ligand positioning and local changes in the MD2 binding cavity during molecular dynamics simulation, representative molecular surfaces of the MD2 pocket were generated from selected trajectory frames. Surface visualization was performed to evaluate the spatial relationship between fumaric acid and the surrounding cavity environment.

The surface was colored according to hydrophobicity, with hydrophilic regions shown in blue and hydrophobic regions shown in brown. Representative conformations from the fumaric acid-bound trajectory were selected to compare changes in ligand location and the surrounding focused on the LPS-binding cavity of MD2, including

ligand migration, cavity accessibility, and local rearrangement of surrounding residues during the simulation.pocket environment. Structural inspection

2.9. Isolation of Primary Human PBMCs

Human peripheral blood samples were obtained from 15 healthy adult male volunteers (age range: 18–23 years) following written informed consent and approval by the institutional review board. Peripheral blood mononuclear cells (PBMCs) were isolated by density gradient centrifugation using Ficoll–Paque Premium according to established procedures[21].

Briefly, heparinized whole blood was diluted with sterile phosphate-buffered saline (PBS) and layered onto Ficoll–Paque Premium. Following centrifugation, the mononuclear cell layer was collected and washed with PBS to remove residual Ficoll and contaminating platelets. Cell viability was assessed using trypan blue exclusion before experimental treatments. Purified PBMCs were resuspended in complete RPMI-1640 medium supplemented with 10% heat-inactivated fetal bovine serum (FBS), 1% penicillin–streptomycin, and 2 mM L-glutamine and maintained at 37°C in a humidified incubator containing 5% CO_2 until stimulation.

2.10. In Vitro Endotoxin Stimulation and Fumaric Acid Co-Treatment

To evaluate the effect of fumaric acid on LPS-induced inflammatory responses, primary human PBMCs were stimulated with purified LPS at a final concentration of 1 μg/mL. Fumaric acid (free acid form) was prepared immediately before treatment and added at concentrations of 10 ng/mL or 100 ng/mL during LPS stimulation.

The experimental groups were configured as follows:

- **Control (Ctrl):** untreated PBMCs.
- **LPS:** PBMCs stimulated with 1 μg/mL LPS alone.
- **F10+LPS:** PBMCs co-treated with 10 ng/mL fumaric acid and 1 μg/mL LPS.
- **F100+LPS:** PBMCs co-treated with 100 ng/mL fumaric acid and 1 μg/mL LPS.

All treatment groups were incubated for 24 h under standard cell culture conditions (37°C, 5% CO_2). Cells were subsequently collected for total RNA extraction, and culture supernatants were collected for cytokine measurement.

2.11. Total RNA Extraction

Total cellular RNA was isolated from treated PBMC samples using the TRIzol reagent extraction method according to the protocol described by Bahari et al. (2017)[22]. Briefly, PBMC pellets were lysed in TRIzol reagent and homogenized. Following chloroform addition and centrifugation, the aqueous phase was collected, and RNA was precipitated using isopropanol. RNA pellets were washed with 70% ethanol, air-dried, and dissolved in nuclease-free water. RNA concentration and purity were assessed by spectrophotometric analysis, and samples with acceptable purity were used for downstream quantitative PCR (qPCR) analysis.

2.12. First-Strand cDNA Synthesis

Complementary DNA (cDNA) was synthesized from 1–2 µg of purified total RNA using a first-strand cDNA synthesis kit with oligo(dT) primers targeting polyadenylated mRNA transcripts, according to the manufacturer's instructions and the method described previously by Bahari et al.[22]. Reverse transcription was performed in a final reaction volume of 40 µL. Following synthesis, cDNA products were diluted with nuclease-free water and stored at −20 °C until quantitative real-time PCR analysis.

2.13. Quantitative Real-Time PCR (qPCR)

Quantitative real-time PCR was performed using SYBR Green master mix chemistry in a final reaction volume of 20 µL. Each reaction contained cDNA template, SYBR Green master mix, and gene-specific forward and reverse primers listed in Table 1, following the protocol described by Bahari et al.[22].

The thermal cycling program consisted of an initial denaturation and enzyme activation step at 95°C for 15 min, followed by 45 amplification cycles. Each cycle included denaturation at 95°C for 20 s, annealing at 55°C for 20 s, and extension at 72°C for 20 s. A melting curve analysis was performed after amplification to confirm product specificity and assess potential primer-dimer formation or non-specific amplification.

Relative expression levels of inflammatory genes, including *IL1B*, *TNF*, and *NFKB1*, were calculated using the comparative $2^{-}\Delta\Delta Ct$ method and normalized to *GAPDH* as the internal reference gene. Each biological sample was analyzed in technical triplicate, with biological replicates obtained from independent donors.

	Target	Fwd & Rev sequences	Amplicon(bp)	T_m (°C)
TLR4 Pathway genes	*NFKB1*	TGCTGGAGTTCAGGATAAC	179 mer	60.7
		GGATGATTGCTAAGTGAGAC		60.7
	TNF	CTCTTCTCCTTCCTGATC	190 mer	50.57
		CTTGAGGGTTTGCTACAA		52.00
	IL1β	CTTTGAAGAAGAACCTATCT	178 mer	49.72
		CACTTGTTGCTCCATATC		50.42
reference	GAPDH	GGTCAGATCCACAACGGACA	196 mer	59.63
		CACTGCCACCCAGAAGACTG		60.42

Table 1. Primer sequences and qPCR conditions for analysis of inflammatory genes associated with TLR4 signaling. The table lists forward and reverse primer sequences, expected amplicon sizes, and primer melting temperatures (Tm) for quantitative real-time PCR analysis of *NFKB1, TNF*, *IL1B*, and *GAPDH*.

2.14. Cytokine Measurement by ELISA

After 24 h of treatment, culture supernatants were collected and IL-1β and TNF-α concentrations were measured by ELISA. Concentrations are reported in pg/mL. Each group comprised three biological and three technical repeats.

2.15. Statistical analysis

Quantitative experimental data are presented as mean ± standard deviation (SD). Statistical analyses were performed using SPSS software. Differences among experimental groups were evaluated using one-way analysis of variance (ANOVA), followed by Tukey's honestly significant difference (HSD) post hoc test for multiple comparisons. Biological replicates obtained from independent donors were considered independent samples for statistical analysis.

A p-value < 0.05 was considered statistically significant. For qPCR, each group comprised four replicates; for ELISA, each group comprised three biological and three technical repeats.

3. Results

3.1. Structure-Based Screening and Consensus Hit Identification

The prepared TCM compound library was screened against the TLR4/MD2 LPS-binding region using sequential Glide docking stages, including high-throughput virtual screening (HTVS), standard precision (SP), and extra precision (XP) docking. Compounds retained after the XP stage were further evaluated by independent re-docking using three additional platforms: MOE, ICM-Pro, and CLC Drug Discovery Workbench to identify candidates with consistent computational prioritization across different scoring approaches.

All 216 hits were capable of forming hydrogen-bond interactions with serine and arginine residues. Average docking scores ranged from −3.69 (mesaconic acid) to −18.99 (ganosporeric acid A), and several compounds had more negative averages than fumaric acid (−5.40). Although fumaric acid was not the highest-ranked compound based solely on averaged docking score, it demonstrated the most consistent cross-platform prioritization, with the lowest score variability among the final candidates (SD 3.27; Table 2), and was therefore prioritized for downstream testing in PBMCs. The cross-platform overlap of the prioritized candidates is shown in the three-way Venn diagram (Figure 2). In addition, only 10 of the prioritized leads passed the conservative ADME/Tox assessment using BIOVIA Discovery Studio 2017.

Lead compound	Source organism(s)	Molecular formula	Maestro score	CLC score	ICM score	MOE score	Average score	SD
Mesaconic acid	*Saccharum sinensis*	$C_5H_6O_4$	-2.83	-8.81	-0.09	-3.04	-3.69	3.67
Fumaric acid	*Plantago major*, *Urtica dioica*	$C_4H_4O_4$	-2.58	-9.52	-6.52	-2.98	-5.40	3.27
Aminozide	*Chrysanthemum morifolium*	$C_6H_{10}N_2O_3$	-3.25	-23.22	1.96	-3.55	-7.01	11.10
Oxaloacetic acid	*Euonymus alatus*	$C_4H_4O_5$	-3.47	-11.19	-13.67	-2.81	-7.79	5.46
Canaline	*Robinia pseudoacacia*	$C_4H_9N_2O_3$	-1.82	-14.68	-15.14	-3.43	-8.77	7.13
Uridine monophosphate	*Agaricus campestris*	$C_8H_{10}N_2O_9P$	-4.44	-30.10	-2.48	-4.25	-10.32	13.22
Allantoic acid	*Wisteria sinensis*	$C_4H_7N_4O_4$	-3.37	-18.68	-20.17	-2.87	-11.27	9.44
Limocitrol	*Citrus* spp.	$C_{18}H_{15}O_9$	-3.39	-30.03	-19.78	-4.48	-14.42	12.82
Mesuaxanthone B	*Mesua ferrea*	$C_{13}H_8O_5$	-1.06	-39.87	-19.70	-3.78	-16.10	17.85
Ganosporeric acid A	*Ganoderma lucidum*	$C_{30}H_{37}O_8$	-7.42	-51.28	-11.68	-5.57	-18.99	21.68

Table 2. Docking scores and natural sources of the prioritized candidate compounds. The table lists the natural source, molecular formula, and docking scores of the ten prioritized leads obtained from multi-platform virtual screening against the TLR4/MD2 complex. For each compound, the best-scoring conformer from Glide, CLC Drug Discovery Workbench, ICM-Pro, and MOE is reported using each program's own scoring units. The Average score

column is the arithmetic mean of the four docking scores and was used for comparative prioritization; the SD column is the descriptive standard deviation of the four scores for each compound.

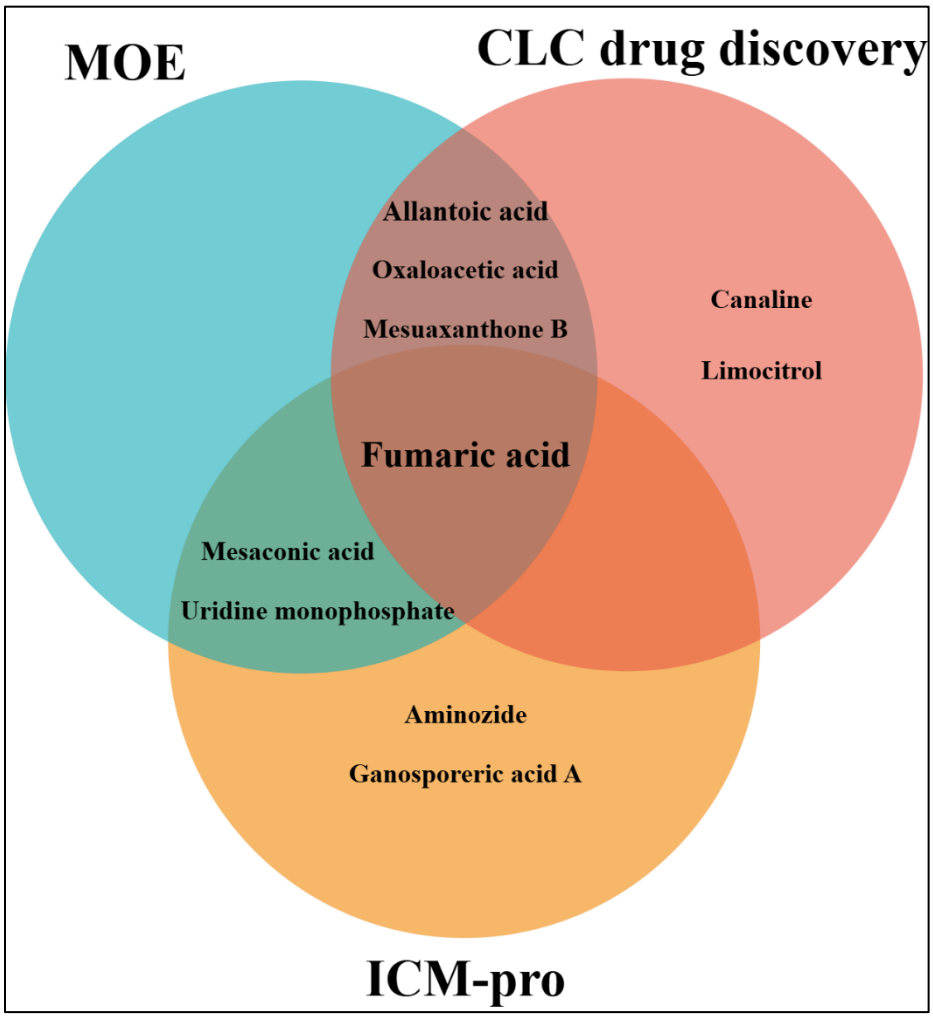

Figure 2. Consensus-based candidate selection across multiple docking platforms. Three-way Venn diagram showing the overlap among candidate compounds identified by MOE, ICM-Pro, and CLC Drug Discovery Workbench after re-docking of XP-ranked compounds against the TLR4/MD2 complex. Compounds located in overlapping regions represent candidates recovered by multiple docking platforms. Fumaric acid was the only compound present in the intersection of all three platforms and was selected for subsequent molecular dynamics simulation and experimental evaluation.

Although the absolute docking scores differed among platforms due to differences in scoring functions and algorithms, fumaric acid showed consistent retention across the evaluated docking approaches. Its arithmetic mean docking score across the four platforms was −5.40, and its selection was further supported by its presence across all three re-docking candidate sets and the lowest descriptive standard deviation among the evaluated compounds. Therefore, fumaric acid was selected for subsequent molecular dynamics simulations and experimental evaluation.

3.2. Atomistic Binding Modes and Static Interaction Landscapes

To characterize the predicted binding orientation of fumaric acid within the MD2 cavity, two-dimensional and three-dimensional interaction analyses were performed using the docking output. The interaction map of fumaric acid (Figure 3A) showed predicted contacts between the ligand carboxylate groups and residues located near the polar region of the MD2 binding cavity. The predicted interaction pattern included hydrogen-bond interactions involving Ser120 and Arg264 (TLR4), together with hydrophobic contacts involving Phe119 and other pocket-lining residues around the alkene region of fumaric acid. In the starting-pose diagram used for the MD simulations (Figure 4B), Ser118 (side chain), Phe119 (backbone) and Ser120 (backbone) formed hydrogen bonds with the carboxylate oxygen atoms. The native LPS ligand from the TLR4/MD2/LPS crystal structure was analyzed as a structural reference (Figure 3B). The interaction patterns of fumaric acid and LPS represent distinct ligand chemotypes occupying the same general MD2 binding region rather than equivalent interaction profiles.

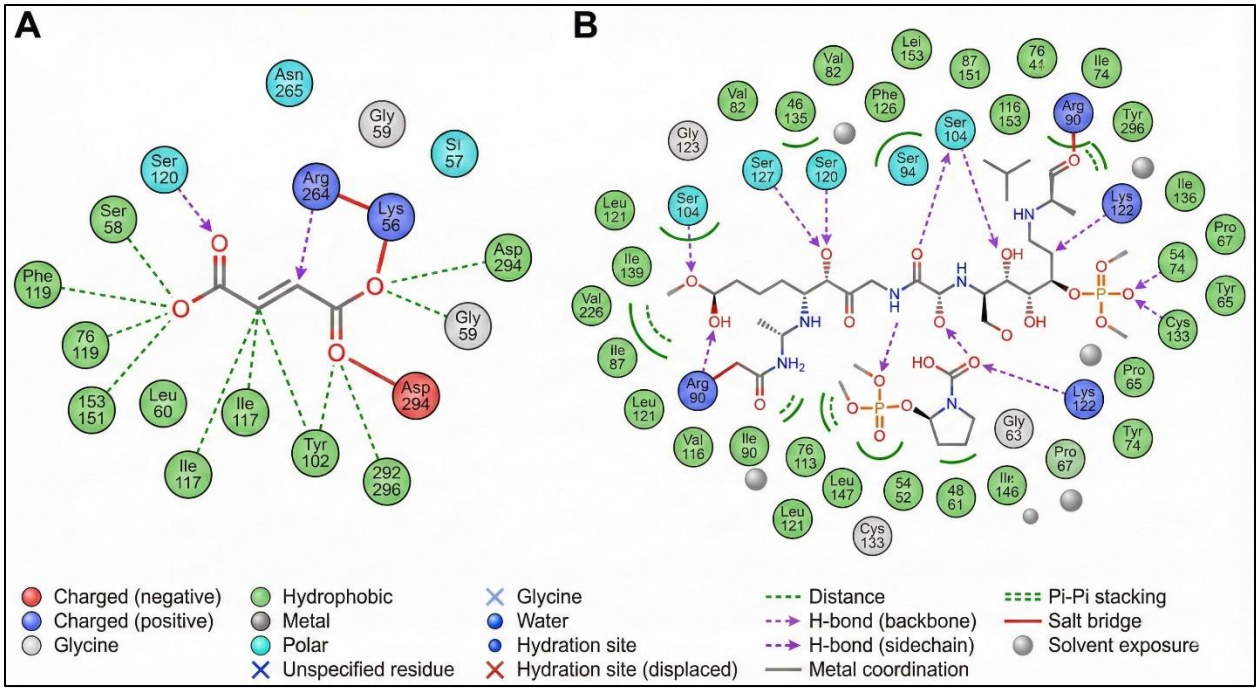

Figure 3. Two-dimensional interaction diagrams of fumaric acid (A) and the native LPS ligand from the 4G8A crystal structure (B) within the TLR4/MD2 complex. Residues are colored according to their physicochemical properties, and the interaction legend is provided in the figure.

Three-dimensional visualization of the docking pose (Figure 4) showed that fumaric acid was positioned near the entrance of the MD2 cavity associated with LPS recognition. The small ligand scaffold was located in proximity to the surrounding pocket residues, while the carboxylate groups remained oriented toward the polar region of the cavity. The displayed ligand orientation and interaction geometry were obtained directly from docking outputs without manual modification or post-docking realignment.

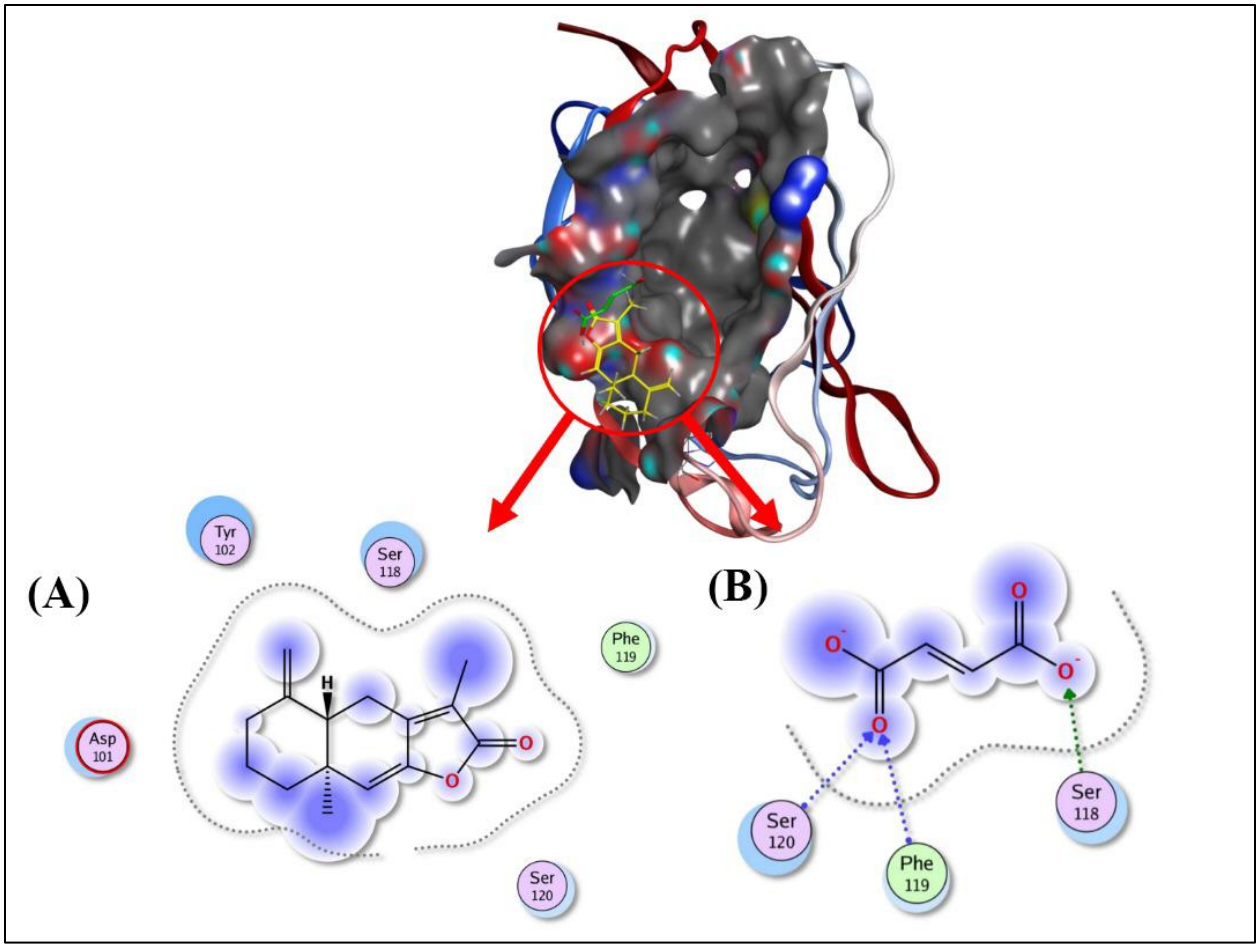

Figure 4. Starting poses of the reference ligand atractylenolide I (A) and fumaric acid (B) at the MD2 binding pocket. The upper panel shows the TLR4/MD2 surface with the ligand positions highlighted, and the lower panels show the local interaction environment of each ligand. In panel B, Ser118, Phe119, and Ser120 are indicated as residues involved in predicted hydrogen-bond interactions with fumaric acid (side-chain hydrogen bond for Ser118; backbone hydrogen bonds for Phe119 and Ser120).

3.3. Hierarchical Clustering by Structural Similarity

To compare the structural relationships among the selected compounds and TLR4/MD2 reference ligands, hierarchical clustering was performed using structural similarity analysis in ICM-Pro (Figure 5). The dendrogram grouped the ten candidate compounds together with native LPS and Eritoran according to their structural similarity relationships.

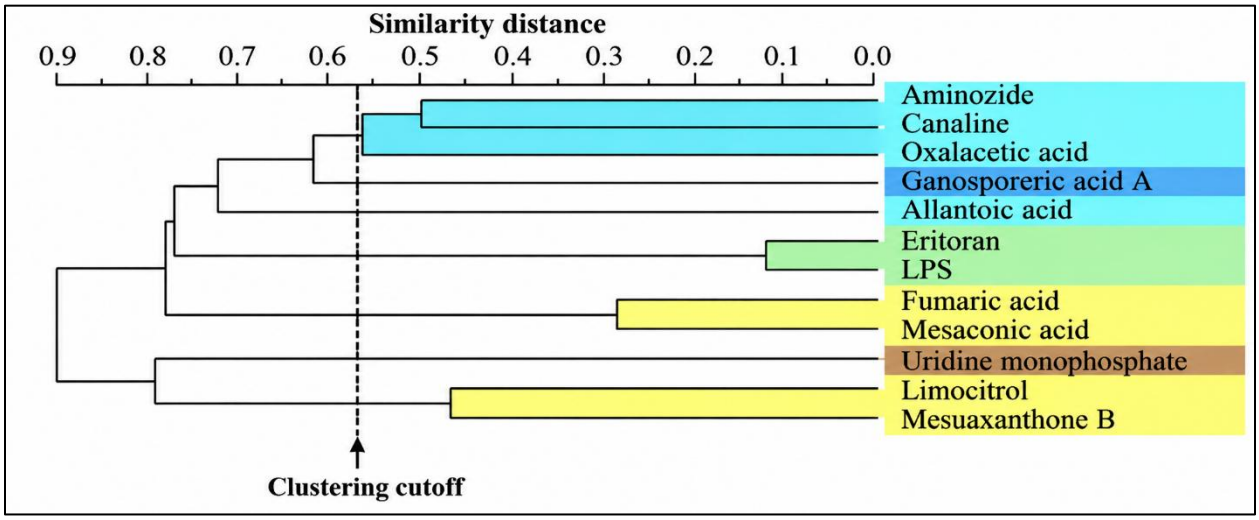

Figure 5. Hierarchical clustering of candidate compounds and TLR4/MD2 reference ligands based on structural similarity. The dendrogram shows similarity relationships among the ten selected compounds together with Eritoran and LPS, generated using hierarchical clustering in ICM-Pro with the unweighted pair group method with arithmetic mean (UPGMA). Branch lengths represent similarity distance (scale 0.9–0.0), and the dashed line indicates the clustering cutoff used to define major groups. Colored regions highlight related compound clusters. Fumaric acid clusters with mesaconic acid, whereas Eritoran and LPS form a separate reference ligand cluster.

Fumaric acid clustered closely with the structurally related dicarboxylic acid mesaconic acid, with a similarity distance of approximately 0.28 (Figure 5). This cluster was separated from the branch containing the lipid-based reference ligands, where LPS and Eritoran formed a close structural pair at a distance of approximately 0.12. The fumaric acid/mesaconic acid cluster joined the LPS/Eritoran branch at a larger distance (approximately 0.78), indicating lower structural similarity between these groups.

Overall, the clustering analysis showed that fumaric acid had greater structural similarity to small organic acid compounds within the evaluated dataset than to the lipid-derived TLR4/MD2 reference ligands. These results provide structural context for the comparison of fumaric acid with known LPS-associated compounds.

3.4. Explicit-Solvent Molecular Dynamics Analysis of Complex Behavior

To evaluate the dynamic behavior of the docked complexes under explicit-solvent simulation conditions, molecular dynamics simulations were performed for 100 ns (100,000 ps). Trajectory analysis revealed distinct conformational behaviors among the simulated systems (Figure 6). Backbone RMSD analysis showed that the apo complex (TLR4-Empty, orange trace) and the atractylenolide-I-bound reference complex (TLR4-Ref-RMSD, blue trace) maintained similar RMSD profiles, mainly within the range of approximately 1.5–2.0 Å. In contrast, the fumaric acid-bound complex (TLR4-FUMA-RMSD, green trace) displayed an initial RMSD increase reaching approximately 5.5 Å, followed by a lower and distinct RMSD profile during the later simulation period. This difference suggests that fumaric acid binding was associated with a distinct conformational trajectory compared with the apo and atractylenolide-I-bound systems, potentially reflecting ligand-associated adaptation within the MD2 pocket.

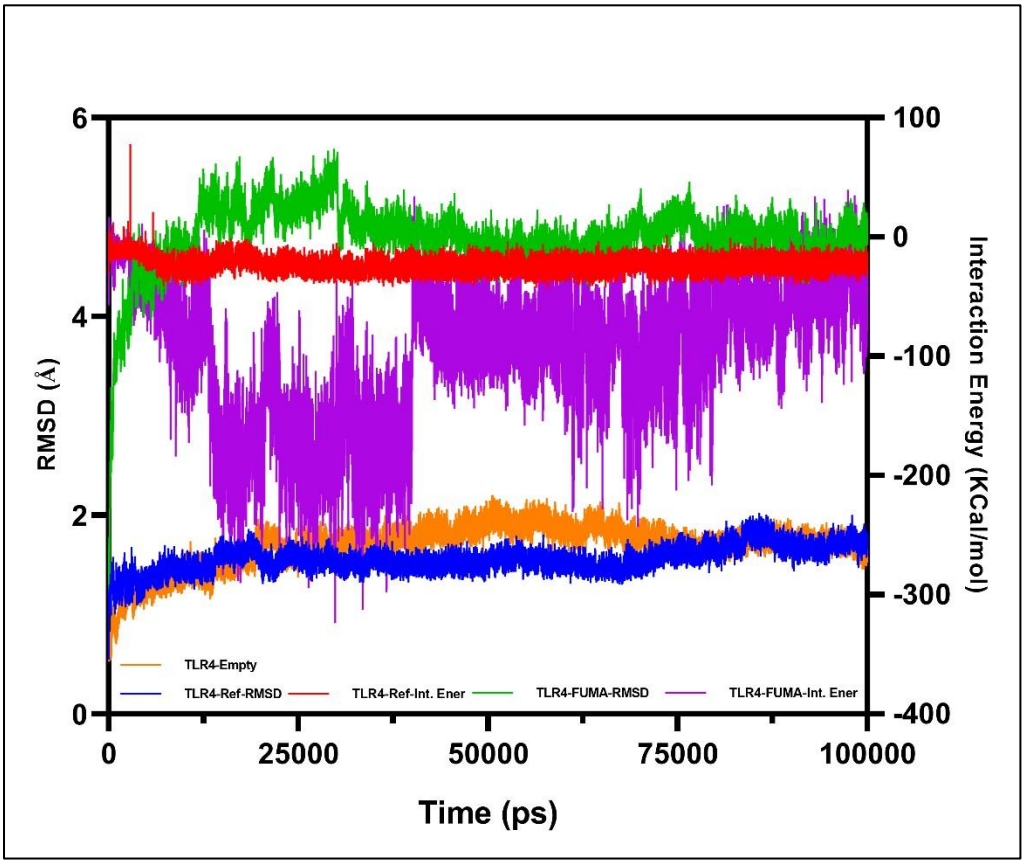

Figure 6. Molecular dynamics trajectory analysis of TLR4/MD2 complexes. Trajectory analysis of 100 ns molecular dynamics simulations of the apo TLR4/MD2 complex (TLR4-Empty), atractylenolide-I-bound complex (TLR4-Ref), and fumaric acid-bound complex (TLR4-FUMA). RMSD profiles (left axis) show temporal changes in backbone conformational behavior, while interaction energy profiles (right axis) represent calculated protein–ligand interaction energies during the trajectory. The fumaric acid-bound complex displayed a distinct RMSD trajectory and a different interaction energy profile compared with the apo and atractylenolide-I reference systems.

The RMSD differences were accompanied by distinct protein–ligand interaction energy profiles (Figure 6). The fumaric acid-bound complex showed an interaction energy of −95.7 ± 56.9 kcal/mol, with large fluctuations reaching approximately −150 to −250 kcal/mol during parts of the trajectory. In comparison, the atractylenolide-I reference complex showed −23.2 ± 6.2 kcal/mol with smaller fluctuations. These values describe different calculated protein–ligand interaction energies between the two ligand-bound systems, with high variability for fumaric acid, and are not binding affinities.

Representative surface conformations extracted from the trajectories were further analyzed to visualize fumaric acid positioning within the MD2 cavity (Figure 7). These structural observations provide additional context for the docking and molecular dynamics analyses.In the initial frame, fumaric acid was located at the protein surface near the entrance of the MD2 cavity (Figure 7A); in a later representative frame, it was positioned within the internal pocket, with changes in ligand orientation and local pocket geometry (Figure 7B), consistent with dynamic accommodation within

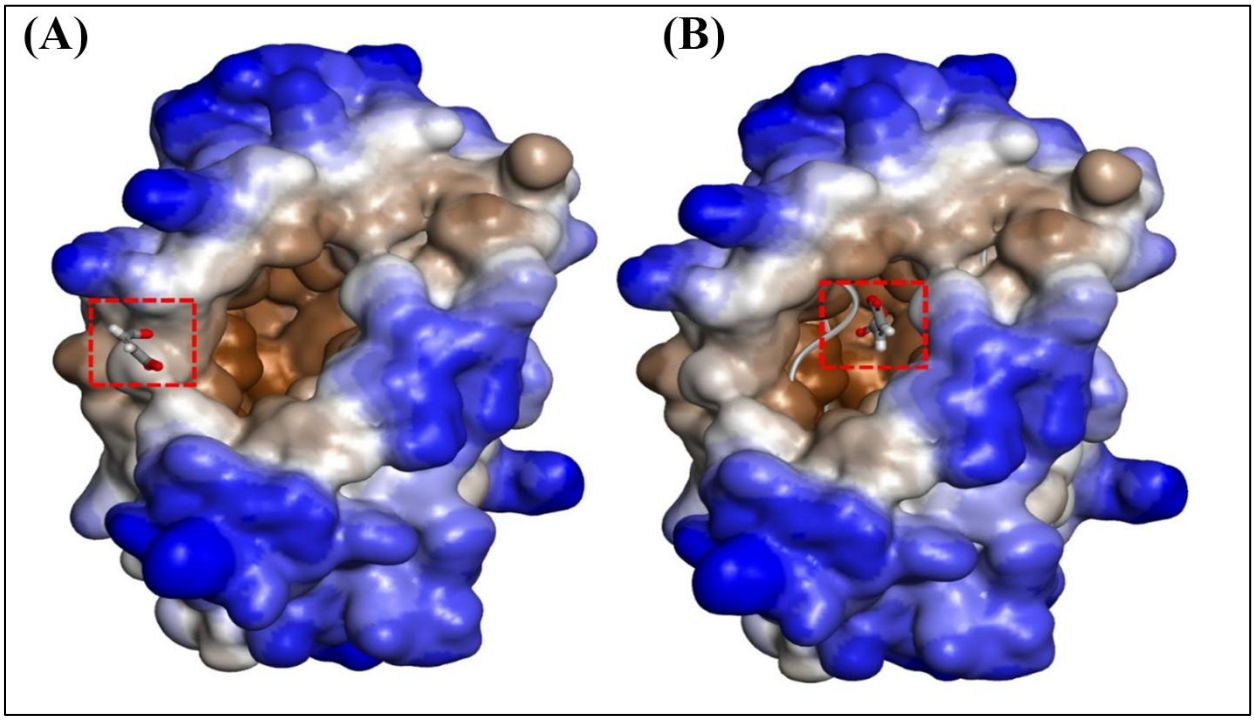

the MD2 binding environment.

Figure 7. Representative molecular dynamics frames showing fumaric acid repositioning within the MD2 binding cavity. Surface representations of the MD2 protein are shown according to the hydrophobicity index, with blue regions indicating more hydrophilic areas and brown regions indicating more hydrophobic areas. (A) Initial position of fumaric acid (dashed box) at the protein surface near the entrance of the deep hydrophobic MD2 cavity. (B) Representative later conformation showing fumaric acid positioned within the internal pocket region, accompanied by changes in the surrounding protein surface conformation. These structural snapshots illustrate ligand repositioning during the simulation and provide additional context for the RMSD and interaction energy analyses.

3.5. Ex Vivo Evaluation of Fumaric Acid Effects on LPS-Induced Inflammatory Responses in Human PBMCs

To evaluate whether the computationally prioritized fumaric acid candidate influenced LPS-induced inflammatory responses, primary human PBMCs were stimulated with purified LPS (1 μg/mL) and co-treated with fumaric acid at two concentrations (Figure 8). Quantitative PCR analysis showed that LPS stimulation significantly increased the expression levels of *IL1B*, *TNF*, and *NFKB1* transcripts compared with untreated control cells ($p < 0.001$ for *IL1B* and *TNF*; $p < 0.01$ for *NFKB1*; Figure 8A). Fumaric acid co-treatment modulated LPS-induced gene expression in a concentration-dependent but gene-specific manner.

At 10 ng/mL (F10+LPS), *IL1B* expression was not significantly different from control, whereas *NFKB1* expression remained significantly elevated ($p < 0.05$; Figure 8A). At 100 ng/mL (F100+LPS), *NFKB1* expression was not significantly different from control, whereas *IL1B* remained significantly elevated ($p < 0.01$; Figure 8A). *TNF* expression remained significantly elevated relative to control at both concentrations ($p < 0.001$), and no significant reduction of *TNF* transcripts was observed. In contrast, TNF-α and IL-1β concentrations in culture supernatants, measured by ELISA, were significantly lower than in the LPS group at both 10 ng/mL and 100 ng/mL fumaric acid ($p < 0.0001$; Figure 8B).

The magnitude of response reduction varied among individual donors, and cytokine production remained detectable after treatment. These findings indicate that fumaric acid attenuated LPS-induced *IL1B* and *NFKB1* expression and cytokine secretion in primary human PBMCs without completely eliminating cytokine production.

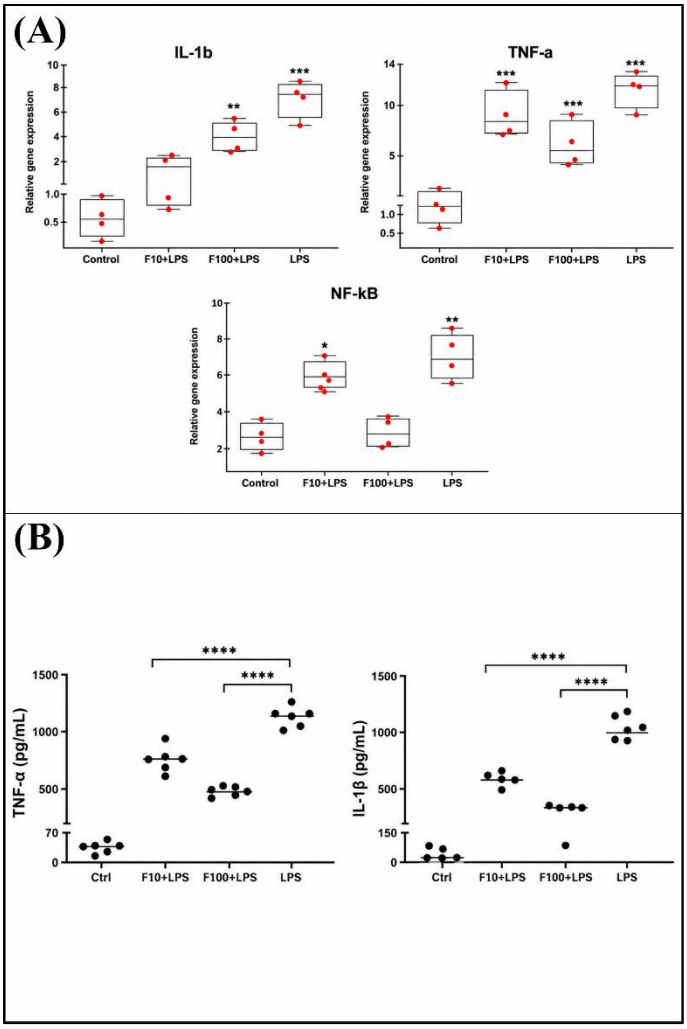

Figure 8. Effect of fumaric acid co-treatment on LPS-induced inflammatory responses in human PBMCs. (A) Relative expression of *IL1B*, *TNF* and *NFKB1* measured by qPCR (n = 4 replicates per group; box plots with individual data points). Asterisks indicate significance versus the untreated control. (B) TNF-α and IL-1β concentrations (pg/mL) in culture supernatants measured by ELISA (six data points per group, comprising three biological and three technical repeats). Brackets indicate comparisons with the LPS group. Human PBMCs were treated with LPS (1 µg/mL) for 24 h and co-treated with fumaric acid at 10 ng/mL (F10+LPS) or 100 ng/mL (F100+LPS); untreated cells served as controls (Ctrl). Data were analyzed by one-way ANOVA followed by Tukey's HSD test. * $p < 0.05$, ** $p < 0.01$, *** $p < 0.001$, **** $p < 0.0001$.

4. Discussion

The present study developed an integrated computational–experimental workflow to prioritize and functionally evaluate a chemically simple small molecule associated with the TLR4/MD2 inflammatory signaling axis. Rather than relying on a single docking score, which may be strongly influenced by the assumptions and scoring functions of individual computational platforms, the screening strategy combined sequential docking refinement, cross-platform

re-docking, consensus selection, structural clustering, molecular dynamics simulation, and primary human cell evaluation (Figure 1). This approach was designed to improve confidence during early-stage candidate prioritization while maintaining appropriate limitations regarding binding affinity and mechanism.

A central finding of this study was that fumaric acid was the only compound consistently recovered across the three independent re-docking platforms used for consensus analysis (Figure 2). This convergence occurred despite substantial differences in absolute scoring ranges among docking engines and despite the presence of compounds that achieved more favorable individual scores within specific platforms (Table 2). Therefore, fumaric acid was not selected because it represented the highest-scoring ligand in every docking environment; rather, it was prioritized because of reproducibility across computational approaches and the lowest cross-platform score variability among the final candidates.

This distinction is important because molecular docking is primarily a structure-guided prioritization method rather than a direct measurement of binding thermodynamics. Docking scores are derived from simplified representations of intermolecular interactions and generally do not account completely for solvent effects, receptor flexibility, entropic contributions, or long-timescale conformational changes. Consequently, docking scores should not be interpreted as experimentally equivalent binding affinities or predictors of biological potency[14]. Within this framework, fumaric acid should be considered a computationally prioritized MD2-pocket-associated candidate rather than a confirmed high-affinity TLR4/MD2 antagonist.

The computational prioritization was further evaluated through two complementary analyses: explicit-solvent molecular dynamics simulations and ex vivo functional assessment in primary human PBMCs. The 100-ns molecular dynamics trajectories demonstrated that the fumaric acid-bound complex maintained a distinct conformational behavior relative to the apo and reference ligand systems, direct receptor binding or quantitative affinity.with negative but strongly fluctuating calculated protein–ligand interaction energies (Figure 6). These findings provide additional information regarding the dynamic accommodation of fumaric acid within the MD2 pocket but do not establish

Importantly, functional evaluation in human PBMCs demonstrated that fumaric acid co-treatment reduced LPS-induced inflammatory responses, including reduced *IL1B* and *NFKB1* transcript levels in a concentration-dependent and gene-specific manner, without a significant reduction of *TNF* transcripts, and reduced secretion of IL-1β and TNF-α under the tested experimental conditions (Figure 8). Taken together, these findings support the interpretation that

fumaric acid represents a small metabolite-like scaffold associated with both computational evidence of MD2-pocket compatibility and measurable attenuation of LPS-induced inflammatory responses in a biologically relevant cellular system. However, these data do not by themselves establish direct TLR4/MD2 antagonism, and the observed cellular effects should be interpreted within the broader context of fumarate biology and immune regulation.

4.1. Structural Basis of MD2 Pocket Accommodation and Predicted Interaction Features

The biological activity of TLR4/MD2 is strongly influenced by ligand-dependent conformational changes within the MD2 binding cavity. Structural studies have demonstrated that the MD2 β-cup fold contains a predominantly hydrophobic internal pocket that accommodates the lipid A component of LPS, while residues located at the cavity entrance contribute to ligand orientation, receptor engagement, and downstream TLR4 dimerization processes[7].

In the present study, docking analysis predicted that fumaric acid occupies a localized region near the polar entrance of the MD2 cavity rather than reproducing the extensive hydrophobic interactions characteristic of lipid A-containing ligands. The two-dimensional interaction analysis showed predicted contacts between fumaric acid and residues surrounding the binding region, including hydrogen-bond interactions involving Ser120 and Arg264 and contacts with charged residues (Figure 3A); in the starting pose used for the MD simulations, Ser118, Phe119 and Ser120 formed hydrogen bonds with the carboxylate groups (Figure 4B). Three-dimensional visualization further demonstrated that fumaric acid was positioned near the entrance of the MD2 cavity with its carboxylate groups oriented toward polar regions of the pocket (Figure 4B).

The predicted interaction pattern differs substantially from the binding mode of native LPS, which contains multiple acyl chains that occupy the hydrophobic cavity and contribute directly to productive TLR4/MD2 complex formation (Figure 3B). Likewise, the interaction mode predicted for fumaric acid is distinct from larger amphiphilic antagonists such as Eritoran, which were designed to occupy the MD2 cavity while preventing productive receptor activation[11]. Therefore, fumaric acid should not be considered a structural mimic of lipid A or a classical MD2 antagonist.

Instead, the predicted binding configuration suggests that a small polar dicarboxylic acid scaffold may influence a restricted region of the MD2 pocket through localized polar contacts and hydrogen bonds. Such interactions could potentially alter local pocket properties; however, the current structural analyses cannot demonstrate complete cavity blockade, interference with LPS transfer mechanisms, or prevention of TLR4 dimerization.

The molecular dynamics surface analysis provides additional structural context for this interpretation. Representative trajectory-derived conformations demonstrated repositioning of fumaric acid from an initial surface-associated location toward the internal MD2 pocket region, accompanied by changes in surrounding surface configuration (Figure 7). These observations suggest that the ligand can adopt alternative positions within the simulated pocket environment and highlight the dynamic nature of the MD2 binding region.

Pocket plasticity is an established feature of TLR4/MD2 biology, particularly for lipid-derived ligands where loop rearrangements and local conformational adaptation influence receptor activation states[7]. The observed fumaric acid-associated structural changes should therefore be interpreted as evidence of dynamic accommodation within the simulated environment rather than direct evidence of receptor inhibition. Nevertheless, the predicted localization of fumaric acid within the MD2 cavity provides a structural hypothesis that is consistent with the reduced inflammatory responses observed experimentally.

4.2. Computational Assessment, Molecular Dynamics Interpretation, and Methodological Considerations

The computational strategy applied in this study was designed to address several recognized limitations of structure-based virtual screening, particularly the dependence of individual scoring functions on simplified interaction models. Consensus agreement across independent docking platforms has been proposed as a useful strategy for reducing false-positive prioritization arising from engine-specific scoring behavior, although it does not replace experimental confirmation of molecular interaction[14]. In the present workflow, the agreement between Glide-based screening and independent re-docking using MOE, ICM-Pro, and CLC Drug Discovery Workbench provided an additional selection criterion beyond the ranking generated by any individual docking algorithm (Figure 2).

Hierarchical clustering further provided structural context for the selected compounds by comparing fumaric acid with other prioritized candidates and TLR4/MD2 reference ligands (Figure 5). Fumaric acid showed greater similarity to the structurally related small organic acid mesaconic acid than to the lipid-derived reference ligands LPS and Eritoran. This observation does not indicate equivalent biological activity; rather, it highlights that fumaric acid represents a chemically distinct scaffold from conventional lipid A-like TLR4 modulators. The clustering analysis therefore supports interpretation of fumaric acid as an atypical candidate requiring independent biological evaluation rather than as a structural analogue of established MD2 ligands.

Molecular dynamics simulations were subsequently used to evaluate whether the docked complexes remained structurally compatible under explicit-solvent conditions. The 100-ns trajectories demonstrated different conformational behaviors among the apo, atractylenolide-I-bound, and fumaric acid-bound complexes (Figure 6). The apo and reference ligand systems showed comparable RMSD profiles, whereas the fumaric acid-bound complex displayed a distinct trajectory characterized by an initial conformational adjustment followed by a sustained alternative RMSD profile. Such behavior may reflect ligand-associated adaptation within the MD2 cavity; however, RMSD differences alone cannot determine whether a ligand interaction is favorable or unfavorable.

The calculated protein–ligand interaction energy profiles provided an additional comparison between fumaric acid and the reference ligand system (Figure 6). The fumaric acid complex showed an interaction energy of −95.7 ± 56.9 kcal/mol compared with −23.2 ± 6.2 kcal/mol for the reference complex, with large fluctuations during the simulation, so the more negative value does not by itself indicate stronger binding. Nevertheless, these values should not be interpreted as experimental binding energies or direct measures of affinity. Interaction energy calculations obtained from molecular dynamics trajectories represent force-field-derived energetic components and do not fully incorporate all thermodynamic contributions, including entropic effects and complete solvent reorganization.

Previous computational studies of ligand–protein systems have emphasized that explicit-solvent simulations can provide valuable information regarding conformational flexibility, ligand accommodation, and interaction persistence beyond static docking predictions[23, 24].

However, limitations associated with force-field accuracy, sampling time, and starting conformations remain important considerations. A 100-ns simulation period is commonly used for evaluating protein–ligand complex behavior, including studies involving TLR4/MD2-related systems[25]. Nevertheless, such simulations remain insufficient to fully capture rare events such as complete ligand dissociation, extensive receptor rearrangements, or long-timescale conformational transitions that may occur beyond the accessible simulation window[26].

Accordingly, the molecular dynamics results presented here support the interpretation that fumaric acid can be dynamically accommodated within the MD2 pocket under the simulated conditions. They do not establish quantitative binding affinity or demonstrate that fumaric acid directly prevents LPS recognition. Additional computational approaches, including comparative free-energy calculations, may provide further ranking information among related compounds; however, methods such as MM/PBSA and MM/GBSA also involve assumptions and limitations that

require careful interpretation[27]. Ultimately, direct experimental measurements of receptor engagement remain necessary to establish the molecular mechanism underlying fumaric acid activity.

4.3. Functional Validation in Primary Human PBMCs and Biological Interpretation

A major strength of the present study is the integration of computational prioritization with functional evaluation in primary human immune cells. Human PBMCs provide a physiologically relevant ex vivo model that preserves donor-derived cellular variability and allows assessment of inflammatory responses within a complex immune environment. Following LPS stimulation, PBMCs showed marked induction of inflammatory transcripts, including *IL1B*, *TNF*, and *NFKB1*, confirming activation of the expected inflammatory response. Co-treatment with fumaric acid modulated these LPS-induced transcriptional responses in a concentration-dependent but gene-specific manner (*IL1B* at 10 ng/mL and *NFKB1* at 100 ng/mL), and reduced secreted IL-1β and TNF-α concentrations (Figure 8).

These findings indicate that fumaric acid attenuated inflammatory responses under the experimental conditions evaluated. However, cellular inflammatory readouts alone cannot distinguish between direct receptor-level effects and indirect intracellular regulatory mechanisms. Establishing direct TLR4/MD2 antagonism requires additional evidence, including biochemical target-engagement measurements using purified receptor components and assessment of proximal signaling events such as adaptor recruitment, IκBα degradation, or NF-κB nuclear translocation[28].

The biological interpretation of fumaric acid activity also requires consideration of the broader fumarate signaling landscape. Fumarate derivatives, particularly dimethyl fumarate (DMF), have established immunomodulatory effects that involve intracellular pathways including KEAP1 modification, NRF2 activation, and metabolic regulation[29]. These mechanisms have been extensively characterized for fumarate esters and their intracellular metabolites, which differ substantially from free fumaric acid in terms of lipophilicity, membrane permeability, and cellular distribution.

Therefore, the inflammatory attenuation observed in PBMCs may reflect multiple possible mechanisms. The computational results support a hypothesis involving association of fumaric acid with the MD2 pocket, whereas the cellular phenotype could also involve intracellular metabolic or redox-associated pathways. These possibilities are not mutually exclusive and should be considered when interpreting the biological activity of small polar metabolites[28, 30]. Importantly, the present study does not distinguish between receptor-proximal and intracellular mechanisms, and further pathway-discrimination experiments will be required.

The translational history of TLR4/MD2-directed compounds further emphasizes the need for careful mechanistic interpretation. Although several TLR4-targeted strategies have shown promising preclinical activity, clinical translation has been complicated by pathway complexity, inflammatory heterogeneity, and differences between experimental models and human disease settings[12, 31, 32]. These challenges highlight the importance of combining computational predictions with biologically relevant validation systems while maintaining appropriate limitations regarding mechanism.

Within this context, the current study should be viewed as a discovery-oriented proof-of-concept rather than a therapeutic claim. The findings demonstrate that a multi-stage computational workflow can identify an unconventional small molecule candidate and connect computational prioritization with measurable changes in human inflammatory responses. Similar integrated approaches combining structure-based screening with cellular validation have been used to advance early-stage immunomodulatory compound discovery[8]. However, studies establishing direct MD2 interaction, such as those incorporating isolated protein binding assays for MD2-targeting compounds, provide a higher level of mechanistic confirmation than achieved here[28].

4.4. Limitations and Future Directions

Several limitations should be considered when interpreting the present findings. First, docking scores generated by different computational platforms should be interpreted cautiously, as they are derived from distinct scoring functions and should not be considered direct measures of experimental binding affinity. Fumaric acid was prioritized based on its consistent retention across multiple docking approaches rather than because it represented the highest-scoring compound in every individual platform (Table 2). This consensus-based strategy reduces dependence on a single scoring function but does not eliminate the intrinsic uncertainty associated with structure-based computational prediction[14].

Second, although molecular dynamics simulations and structural analyses supported dynamic accommodation of fumaric acid within the MD2 pocket (Figures 6 and 7), these approaches cannot establish direct biochemical binding or quantify experimental binding thermodynamics. Molecular dynamics provides valuable insights into conformational adaptation and interaction persistence but remains limited by force-field accuracy, finite sampling timescales, and dependence on the initial structural model[24]. Longer simulations and enhanced sampling approaches may therefore be required to capture rare conformational transitions or alternative ligand-binding states[26].

Third, the present study did not include direct biochemical target-engagement assays using purified MD2 protein or TLR4/MD2 complexes. Therefore, the PBMC findings should be interpreted as evidence of reduced LPS-associated inflammatory responses rather than definitive proof of direct MD2 receptor antagonism. Previous studies of MD2-targeting compounds have demonstrated the importance of integrating cellular inflammatory assays with complementary mechanistic validation approaches, including direct protein–ligand interaction analyses, to establish target-associated activity[28]. Finally, fumarate-derived molecules have recognized roles in immunometabolic regulation, including protein modification and metabolic reprogramming pathways that influence inflammatory immune responses[29]. Although the computational results support a hypothesis involving fumaric acid association with the MD2 pocket, the cellular phenotype may also involve intracellular regulatory mechanisms. Future studies comparing free fumaric acid with fumarate derivatives, incorporating pathway-discrimination experiments, and directly measuring MD2 engagement will be necessary to distinguish receptor-associated effects from alternative immunometabolic mechanisms.

4.5. Conclusion and Perspective

The present study establishes an integrated computational–experimental workflow combining sequential docking refinement, multi-platform consensus analysis, structural comparison, molecular dynamics simulation, and evaluation in primary human PBMCs (Figure 1). This strategy enabled identification of fumaric acid as an unconventional MD2-pocket-associated candidate through reproducible computational prioritization rather than reliance on a single docking score.

The computational analyses suggest that fumaric acid can occupy a region of the MD2 binding environment and be dynamically accommodated there during simulation. The biological experiments further demonstrate that fumaric acid reduces LPS-induced *IL1B* and *NFKB1* expression and IL-1β and TNF-α secretion in primary human PBMCs under the tested conditions (Figure 8). However, the current evidence supports functional inflammatory attenuation and a predicted MD2-associated interaction model rather than definitive identification of fumaric acid as a direct TLR4/MD2 antagonist.

Future studies should focus on direct biochemical validation of MD2 engagement, mechanistic separation of receptor-associated and intracellular fumarate pathways, and comparative evaluation of structurally related compounds. Such

investigations will clarify whether small metabolite-like scaffolds can represent a distinct class of modulators within the complex biology of LPS–TLR4/MD2 signaling.

Despite these limitations, the present study provides a systematic framework for integrating structure-based computational prioritization with functional immunological evaluation to identify chemically unconventional candidates associated with LPS-induced inflammatory regulation. Through multi-platform docking consensus, molecular dynamics assessment, and validation in primary human PBMCs, fumaric acid emerged as a candidate small-molecule scaffold associated with reduced inflammatory responses under the tested conditions. However, the current findings should be regarded as a foundation for further mechanistic investigation rather than as evidence of definitive TLR4/MD2 antagonism. Future studies incorporating direct target-engagement approaches, pathway-discrimination experiments, and comparative evaluation of related fumarate-derived structures will be essential to determine whether the observed activity arises primarily from MD2-associated interactions, intracellular immunometabolic regulation, or a combination of both mechanisms. Such investigations will clarify the biological relevance of small metabolite-like compounds in modulating complex innate immune signaling pathways and may expand strategies for discovering atypical regulators of TLR4/MD2-associated inflammation.

Acknowledgments

The authors would like to express their sincere gratitude to Saeed Razzaghi at the Information Technology Center, University of Zanjan, for his valuable technical support and assistance during this project.

Declarations of interest: none**.**

References

1. Rudd, K.E., et al., *Global, regional, and national sepsis incidence and mortality, 1990-2017: analysis for the Global Burden of Disease Study.* Lancet, 2020. **395**(10219): p. 200-211.
2. Ohto, U., et al., *Structural analyses of human Toll-like receptor 4 polymorphisms D299G and T399I.* J Biol Chem, 2012. **287**(48): p. 40611-7.
3. Ain, Q.U., M. Batool, and S. Choi, *TLR4-Targeting Therapeutics: Structural Basis and Computer-Aided Drug Discovery Approaches.* Molecules, 2020. **25**(3).
4. Lami, F., et al., *Validating Natural Compounds as Toll-Like Receptor 4 (TLR4) Antagonists: Experimental Challenges and Therapeutic Perspectives.* J Med Chem, 2026. **69**(1): p. 72-86.

5. Kim, H.J., et al., *Toll-like receptor 4 (TLR4): new insight immune and aging*. Immun Ageing, 2023. **20**(1): p. 67.
6. Fu, Y., et al., *Structural insight into TLR4/MD-2 activation by synthetic LPS mimetics with distinct binding modes*. Nat Commun, 2025. **16**(1): p. 4164.
7. Park, B.S., et al., *The structural basis of lipopolysaccharide recognition by the TLR4-MD-2 complex*. Nature, 2009. **458**(7242): p. 1191-5.
8. Švajger, U., et al., *Novel toll-like receptor 4 (TLR4) antagonists identified by structure- and ligand-based virtual screening*. Eur J Med Chem, 2013. **70**: p. 393-9.
9. Shimazu, R., et al., *MD-2, a molecule that confers lipopolysaccharide responsiveness on Toll-like receptor 4*. J Exp Med, 1999. **189**(11): p. 1777-82.
10. Zhu, J. and C. Mohan, *Toll-like receptor signaling pathways--therapeutic opportunities*. Mediators Inflamm, 2010. **2010**: p. 781235.
11. Kim, H.M., et al., *Crystal structure of the TLR4-MD-2 complex with bound endotoxin antagonist Eritoran*. Cell, 2007. **130**(5): p. 906-17.
12. Opal, S.M., et al., *Effect of eritoran, an antagonist of MD2-TLR4, on mortality in patients with severe sepsis: the ACCESS randomized trial*. Jama, 2013. **309**(11): p. 1154-62.
13. Kuzmich, N.N., et al., *TLR4 Signaling Pathway Modulators as Potential Therapeutics in Inflammation and Sepsis*. Vaccines (Basel), 2017. **5**(4).
14. Kitchen, D.B., et al., *Docking and scoring in virtual screening for drug discovery: methods and applications*. Nat Rev Drug Discov, 2004. **3**(11): p. 935-49.
15. Chen, C.Y.-C., *TCM Database@Taiwan: The World's Largest Traditional Chinese Medicine Database for Drug Screening In Silico*. PLOS ONE, 2011. **6**(1): p. e15939.
16. Friesner, R.A., et al., *Glide: a new approach for rapid, accurate docking and scoring. 1. Method and assessment of docking accuracy*. J Med Chem, 2004. **47**(7): p. 1739-49.
17. ULC, C.C.G., *Molecular Operating Environment (MOE)*. 2026, Chemical Computing Group ULC: Montreal, QC.
18. Abagyan, R., M. Totrov, and D. Kuznetsov, *ICM—A new method for protein modeling and design: Applications to docking and structure prediction from the distorted native conformation*. Journal of Computational Chemistry, 1994. **15**(5): p. 488-506.
19. QIAGEN, *QIAGEN CLC Drug Discovery Workbench User Manual*. 2023, QIAGEN: Aarhus, Denmark.
20. Zheng, G., et al., *Periodic hierarchical load balancing for large supercomputers*. The International Journal of High Performance Computing Applications, 2011. **25**(4): p. 371-385.
21. Bahari, A. and V. Salmani, *Environmentally relevant dose of arsenic interferes in functions of human monocytes derived dendritic cells*. Toxicol Lett, 2017. **275**: p. 118-122.
22. Bahari, A., et al., *Cytochrome P450 isoforms are differently up-regulated in aflatoxin B_1-exposed human lymphocytes and monocytes*. Immunopharmacol Immunotoxicol, 2014. **36**(1): p. 1-10.
23. Amaro, R.E., et al., *Ensemble Docking in Drug Discovery*. Biophys J, 2018. **114**(10): p. 2271-2278.

24. De Vivo, M., et al., *Role of Molecular Dynamics and Related Methods in Drug Discovery.* J Med Chem, 2016. **59**(9): p. 4035-61.
25. Matamoros-Recio, A., et al., *Full-Atom Model of the Agonist LPS-Bound Toll-like Receptor 4 Dimer in a Membrane Environment.* Chemistry – A European Journal, 2021. **27**(62): p. 15406-15425.
26. Evangelista Falcon, W., et al., *Ensemble Docking in Drug Discovery: How Many Protein Configurations from Molecular Dynamics Simulations are Needed To Reproduce Known Ligand Binding?* J Phys Chem B, 2019. **123**(25): p. 5189-5195.
27. Genheden, S. and U. Ryde, *The MM/PBSA and MM/GBSA methods to estimate ligand-binding affinities.* Expert Opin Drug Discov, 2015. **10**(5): p. 449-61.
28. Wang, Y., et al., *Curcumin Analog L48H37 Prevents Lipopolysaccharide-Induced TLR4 Signaling Pathway Activation and Sepsis via Targeting MD2.* J Pharmacol Exp Ther, 2015. **353**(3): p. 539-50.
29. Kornberg, M.D., et al., *Dimethyl fumarate targets GAPDH and aerobic glycolysis to modulate immunity.* Science, 2018. **360**(6387): p. 449-453.
30. Guberovic, I. and C. Frezza, *Functional implications of fumarate-induced cysteine succination.* Trends in Biochemical Sciences, 2024. **49**(9): p. 775-790.
31. Monnet, E., et al., *Evidence of NI-0101 pharmacological activity, an anti-TLR4 antibody, in a randomized phase I dose escalation study in healthy volunteers receiving LPS.* Clin Pharmacol Ther, 2017. **101**(2): p. 200-208.
32. Anwar, M.A., et al., *Recent clinical trends in Toll-like receptor targeting therapeutics.* Med Res Rev, 2019. **39**(3): p. 1053-1090.

Statements and Declarations

Funding

The authors declare that no funds, grants, or other support were received during the preparation of this manuscript.

Author Contributions

Mobina Azimi: Conceptualization; Methodology; Formal analysis; Resources; Writing – original draft.

Abbas Bahari: Conceptualization; Methodology; Formal analysis; Resources; Project administration; Supervision; Visualization; Writing – original draft; Writing – review & editing.

Bahram Maleki: Conceptualization; Methodology; Formal analysis; Resources; Writing – original draft.

Milad Lagzian: Conceptualization; Formal analysis; Validation; Writing – original draft.

Mahdi Tavakolizadeh: Conceptualization; Methodology; Formal analysis; Investigation; Resources; Validation; Supervision; Writing – original draft; Writing – review & editing.

Davood Kolivand: Conceptualization; Methodology; Formal analysis; Investigation; Resources; Validation; Supervision; Writing – original draft; Writing – review & editing.

Parsa Dorani: Methodology; Investigation; Writing – original draft; Writing – review & editing.

Elahe Gholamian and Fatemeh Seyed Monfared Zanjani: Methodology; Writing – original draft; Writing – review & editing.

Fatemeh Najafi: Investigation; Resources; Writing – original draft.

All authors read and approved the final version of the manuscript.

Ethics approval

This study was conducted in strict accordance with the ethical standards of the institutional research committee and the 1964 Declaration of Helsinki and its later amendments or comparable ethical standards. Experimental protocols involving primary human peripheral blood mononuclear cells (PBMCs) were reviewed and officially approved by the Institutional Review Board (IRB) / Ethics Committee of the University of Zanjan under the assigned ethics approval code IR.ZNU.REC.1402.008.

Consent to participate

Informed consent was obtained from all individual participants included in the study.

Data availability

All data generated or analyzed during this study are included in this article. Additional data are available from the corresponding author upon reasonable request.